

# Fault Tolerant Backstepping Control for Double-Stage Grid-Connected Photovoltaic Systems using Cascaded H-Bridge Multilevel Inverters

H. Katir<sup>1</sup>, A. Abouloifa<sup>1</sup>, K. Noussi<sup>1</sup>, I. Lachkar<sup>2</sup>, A. El Aroudi<sup>3</sup>,  
M. Aourir<sup>1</sup>, F. El Otmani<sup>1</sup>, and F. Giri<sup>4</sup>

**Abstract**—This paper introduces a complete DC-AC conversion system fed by photovoltaic (PV) energy. The system consists of  $N$  PV panels,  $N$  DC-DC boost converters,  $N$  cascaded H-bridge inverters, a DC-link composed of  $N$  capacitors and an LCL filter. This work aims at reaching threefold control objectives: i) Extracting the available maximum power by regulating the voltages across the PV panels, ii) Ensuring a unitary power factor, iii) Regulating the DC-link voltage to a desired reference. To achieve the mentioned objectives, a multi-loop regulator is designed. The PV panels are individually controlled to track the maximum power point in order to efficiently operate at either the same or different varying climatic conditions without failures. In addition to the maximum power point tracking (MPPT) controller, two cascaded loops guaranteeing a satisfactory power factor and DC-link voltage regulation are developed. The nonlinear backstepping approach combined with Lyapunov theory are used based on the averaged model for the synthesis of the multi-loop controller. The performance of the studied system is tested via MATLAB / SimPowerSystems environment. The obtained simulation results prove that the proposed controller meets its objectives and demonstrate the efficiency of the chosen control strategy under faulty conditions.

## I. INTRODUCTION

Power conversion systems relying on photovoltaic (PV) energy have garnered interest because they enable reducing the use of fossil fuels, and thus, lessen environmental pollution. To ensure an appropriate utilization of these clean promising solutions and make use of the energy available across the PV generators via injecting it into the grid, it is necessary to link them to DC-AC converters [1]. Despite the fact that there are numerous converters' topologies used with PVs, multilevel ones present a host of advantages especially when it comes to working with high power applications. Among these highly beneficial multilevel topologies, Cascaded H-Bridge Multilevel Inverters (CHBMs) are widely known to be very effective at injecting low THD current

into the grid [2], [3].

In literature, there exists many research studies that discuss the problem of power conversion using H-bridge inverters. In [4], authors discuss a single stage CHBMI for grid-connected photovoltaic systems. The study focused on a control technique called the modified ripple-correlation control maximum power point tracking (MRCC-MPPT) to rapidly reach the MPP in shading irradiance and decrease the PV voltage harmonic filter in the DC-link voltage controller. Authors in [5] used the sliding mode control technique in an 11-levels CHBMI for an uninterruptible power supply (UPS) application.

This paper focuses on the study and control of the system represented by figure 1. The main contributions of this work are summarized in the following points:

- The regulation of the DC-link to guarantee an appropriate operation of the CHBMI.
- The generation of  $2N + 1$  voltage levels out of the CHBMI which leads to a close to a sinusoidal waveform and thus reducing the dimensions of the LCL filter.
- The injection of a low THD current into the grid.
- The verification of the controlled system fault tolerance abilities.

This work deals with the control of the general DC-AC conversion chain supplied by PV panels. In this paper, a multi-loop backstepping controller is designed for its tracking ability, low transition time and robustness. Additionally, the behavior of the chosen system is investigated within  $N$  PV energy sources under different tests. First, we test the performance of the overall system under standard conditions, then we check its behavior when the PV modules are working under mismatching conditions and lastly we evaluate its performance under faulty conditions, keeping the system working even if any of the input sources fail.

The rest of this paper is organized as follows: Section II presents the system description and mathematical model. Section III covers the controller design. The simulation results are presented in Section IV. Finally, Section V draws some conclusions.

## II. SYSTEM DESCRIPTION AND MODELING

### A. System Description

In this study, we deal with a whole DC-AC conversion system which enables the injection of power into the grid.

\*This work was not supported by any organization

(Corresponding author: Hanane KATIR)

<sup>1</sup>H. Katir, A. Abouloifa, K. Noussi, M. Aourir and F. El Otmani are with TI Lab, Faculty of Sciences Ben M'sik, University Hassan II of Casablanca, BP 7955 Casablanca, Morocco (e-mail: katir.hanane@gmail.com).

<sup>2</sup>I. Lachkar is with ESE Lab, ENSEM of Casablanca, University Hassan II of Casablanca, BP 7955 Casablanca, Morocco (e-mail: lachkaribtisam@gmail.com).

<sup>3</sup>A. El Aroudi is with Department of Electronics, Electrical Engineering and Automatic Control, Universitat Rovira i Virgili, 43002 Tarragona, Spain (e-mail: abdelali.elaroudi@urv.cat).

<sup>4</sup>F. Giri is with NORMANDIE UNIV, UNICAEN, ENSICAEN, LAC, 14000 Caen, France (e-mail: foudgiri@yahoo.fr).

This system can be divided into three major subsystems: The first subsystem includes  $N$  PV panels and  $N$  DC-DC boost converters, the second one contains the DC-link capacitors and the last subsystem is formed by  $N$  cascaded H-bridges, an  $LCL$  filter and the electrical grid. The schematic diagram of the complete system is depicted in Fig.1. The cascaded H-Bridge multilevel inverter is able to generate a multilevel output voltage close to a sinusoidal one providing as many levels as needed depending on the number of inverter's cells, with respect to the following equation:

$$N_{level} = 2N + 1, \quad (1)$$

where  $N$  is the number of H-bridge inverters.

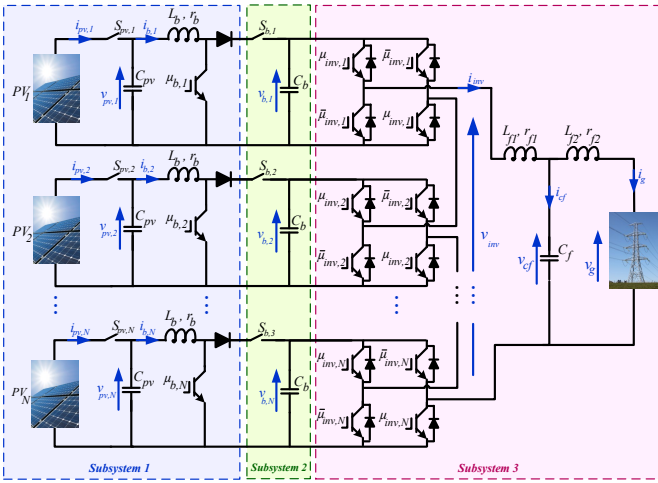


Fig. 1. Scheme of the studied system

### B. System Modeling

The switched mathematical model describing the three subsystems under investigation can be obtained by applying the standard Kirchhoff's laws leading to the nonlinear differential equations (2), (3) and (4); with  $k = 1, 2, \dots, N$ .

$$C_{pv} \frac{dv_{pv,k}}{dt} = i_{pv,k} - i_{b,k}, \quad (2a)$$

$$L_b \frac{di_{b,k}}{dt} = -r_b i_{b,k} + v_{pv,k} - (1 - \mu_{b,k}) v_{b,k}, \quad (2b)$$

Subsystem 2

$$C_b \frac{dv_{b,k}}{dt} = (1 - \mu_{b,k}) i_{b,k} - \mu_{inv,k} i_{inv}, \quad (3)$$

Subsystem 3

$$L_{f_2} \frac{di_g}{dt} = -r_{f_2} i_g + v_{cf} - v_g, \quad (4a)$$

$$C_f \frac{dv_{cf}}{dt} = i_{inv} - i_g, \quad (4b)$$

$$L_{f_1} \frac{di_{inv}}{dt} = -r_{f_1} i_{inv} + \sum_{k=1}^N \mu_{inv,k} v_{b,k} - v_{cf}, \quad (4c)$$

where  $v_{pv,k}$  and  $i_{pv,k}$  are the voltage and current of the  $k^{th}$  PV panel,  $v_{b,k}$  and  $i_{b,k}$  are the voltage and the current of the  $k^{th}$  DC-DC boost converter,  $v_g$  is the grid voltage given

by:  $v_g = E \sin(\omega t)$ .  $i_g$  denotes the grid current,  $v_{inv}$  and  $i_{inv}$  represent the CHBMI voltage and current,  $v_{cf}$  is the voltage across the filter's capacitor,  $\mu_{inv,k} \in \{-1, 1\}$  and  $\mu_{b,k} \in \{0, 1\}$  are the switching signals of the  $k^{th}$  H-bridge inverter and the switching signals of the  $k^{th}$  DC-DC boost converter, respectively.

The mathematical model in (2), (3) and (4) cannot be used to develop appropriate control laws due to the existence of the binary control laws  $\mu_{b,k}$  and  $\mu_{inv,k}$ . Consequently, the following averaged model will be used:

Subsystem 1

$$C_{pv} \dot{x}_{1,k} = i_{pv,k} - x_{2,k}, \quad (5a)$$

$$L_b \dot{x}_{2,k} = -r_b x_{2,k} + x_{1,k} - (1 - u_{b,k}) x_{3,k}, \quad (5b)$$

Subsystem 2

$$C_b \dot{x}_{3,k} = (1 - u_{b,k}) x_{2,k} - u_{inv,k} x_6, \quad (6)$$

Subsystem 3

$$L_{f_2} \dot{x}_4 = -r_{f_2} x_4 + x_5 - v_g, \quad (7a)$$

$$C_f \dot{x}_5 = x_6 - x_4, \quad (7b)$$

$$L_{f_1} \dot{x}_6 = -r_{f_1} x_6 + \sum_{k=1}^N u_{inv,k} x_{3,k} - x_5, \quad (7c)$$

where  $x_{1,k}$ ,  $x_{2,k}$ ,  $x_{3,k}$ ,  $x_4$ ,  $x_5$ ,  $x_6$ ,  $u_{inv,k}$  and  $u_{b,k}$  designate the average values of the signals  $v_{pv,k}$ ,  $i_{b,k}$ ,  $v_{b,k}$ ,  $i_g$ ,  $v_{cf}$ ,  $i_{inv}$ ,  $\mu_{inv,k}$  and  $\mu_{b,k}$ , respectively, over the switching period  $T_s$ .

### III. CONTROLLER DESIGN

The design of the nonlinear controller is performed considering the nonlinear nature of the system and in order to achieve the control objectives. The regulator is developed within three control units aiming at reaching three objectives simultaneously.

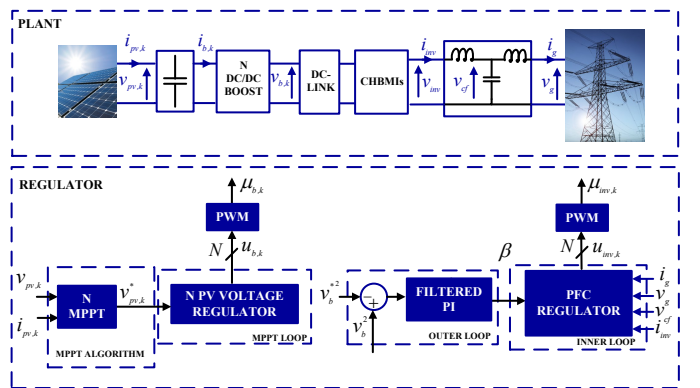


Fig. 2. Block diagram of the controlled system

Our main concern starts with ensuring that the PV panels work in the maximum power points (MPPs). To achieve this objective, it is required to use an MPPT algorithm and to regulate the voltage across each photovoltaic source. We also seek at regulating the DC-link voltages, in a way that they deliver DC voltages to the CHBMI. The fulfilment of this

control objective can be done using a filtered PI regulator; and most importantly, we desire to control the injected grid current to satisfy a unitary power factor (UPF). The developed controller used to achieve the above objectives includes numerous loops, described below:

- $N$  voltage loops ensuring the extraction of the maximum power points of each PV module.
- A current loop that forces the grid current to have the same shape as the grid voltage.
- An outer-loop to control the voltages across the DC-link.

#### A. PV voltage regulator design (MPPT objective)

In order to be able to extract the maximum available power, it is essential to control the PV operating voltage to be around the maximum power point (MPP). There exist numerous MPP extraction techniques that can be used. However, the renowned P&O “perturb and observe algorithm” is the simplest as it only needs the PV voltage and current as inputs to deliver a PV reference voltage in the output to be used later by the DC-DC boost converter [6], [7]. The P&O algorithm guarantees every solar panel to generate a DC voltage close to its MPPs. The uniqueness of the structure presented in this study enables the used solar panels to work at different irradiations/temperatures without facing any problem since they are controlled individually to generate power energy at either similar or mismatching MPPs. This feature is highly important since it allows the system to keep working under the faulty mode as long as at least one PV panel generates energy. It is certain that while facing a failure (either in the PV sources or in the DC-DC boost converters), the generated power is less than the one provided in the normal mode. However, all the control objectives (MPPT, DC-link regulation, PFC) are achieved thanks to the controlled system’s failure tolerance. The output of the PVs feed the DC-DC boost converters which increase the voltage level that would be delivered to the DC-link and then to the CHBML. Since there are  $N$  DC-DC boost converters aiming at stepping-up the PV voltage, it is necessary to control them using an appropriate technique. The proposed control technique that enables the fulfilment of the mentioned objective is the backstepping approach synthesized in two steps since the relative degree of *Subsystem 1* is two.

##### Step 1

It is a necessity to introduce the first tracking error enabling the attainability of the control laws as follows:

$$e_{1,k} = C_{pv}(x_{1,k} - x_{1,k}^*). \quad (8)$$

Equations (5a) and (8) are used to obtain the time-derivation of the first tracking error written as:

$$\dot{e}_{1,k} = i_{pv,k} - x_{2,k} - C_{pv}\dot{x}_{1,k}^*. \quad (9)$$

The following Lyapunov candidate is chosen in a way that it is positive and its time derivative is negative:

$$V_{1,k} = 0.5 e_{1,k}^2. \quad (10)$$

Our choice is made as:

$$\dot{V}_{1,k} = e_{1,k}\dot{e}_{1,k} = -\xi_{1,k}e_{1,k}^2 < 0, \quad (11)$$

where  $\xi_{1,k}$  is a positive design parameter.

Taking into consideration that  $x_{2,k}$  is the  $k^{th}$  virtual control input signal and using the Lyapunov function  $V_{1,k}$  and its dynamics in (10) and (11), the  $k^{th}$  stabilizing function of the subsystem (5a) is expressed as follows:

$$x_{2,k}^* = \xi_{1,k}e_{1,k} + i_{pv,k} - C_{pv}\dot{x}_{1,k}^*. \quad (12)$$

Starting from the fact that  $x_{2,k}$  is not the actual control law and so as to find the final control laws needed to stabilize the subsystems (5a) and (5b), we define the second tracking error:

$$e_{2,k} = L_b(x_{2,k} - x_{2,k}^*). \quad (13)$$

Replacing (9) with (12) and (13), we get:

$$\dot{e}_{1,k} = -\xi_{1,k}e_{1,k} - e_{2,k}/L_b. \quad (14)$$

Accordingly, we deduce the new form of the time derivative of the Lyapunov function as:

$$\dot{V}_{1,k} = -\xi_{1,k}e_{1,k}^2 - e_{1,k}e_{2,k}/L_b. \quad (15)$$

##### Step 2

In order to achieve the final control laws responsible of regulating the voltages across the PV generators as well as boosting the PV’s output voltages, the tracking errors  $e_{1,k}$  and  $e_{2,k}$  must converge to zero.

Let us introduce the dynamics of the second tracking error based on equations (5b) and (13):

$$\dot{e}_{2,k} = -r_b x_{2,k} + x_{1,k} - (1 - u_{b,k})x_{3,k} - L_b\dot{x}_{2,k}^*. \quad (16)$$

The augmented Lyapunov candidate is chosen as follows:

$$V_{2,k} = 0.5e_{2,k}^2 + V_{1,k}. \quad (17)$$

Replacing (15) in the dynamics of (17), the time derivative of the augmented Lyapunov function is written as:

$$\dot{V}_{2,k} = -\xi_{1,k}e_{1,k}^2 - \frac{e_{1,k}e_{2,k}}{L_b} + e_{2,k}\dot{e}_{2,k}. \quad (18)$$

The following condition ensures the negativity of the time derivative of the augmented Lyapunov function candidate:

$$\dot{e}_{2,k} - e_{1,k}/L_b = -\xi_{2,k}e_{2,k} < 0, \quad (19)$$

where  $\xi_{2,k}$  are positive design parameters.

Using equations (16) and (19), the final control laws stabilizing (5a) and (5b) can be expressed as follows:

$$u_{b,k} = 1 + \frac{1}{x_{3,k}} \left( r_b x_{2,k} - \xi_{2,k} e_{2,k} - x_{1,k} + L_b \dot{x}_{2,k}^* + \frac{e_{1,k}}{L_b} \right). \quad (20)$$

**Proposition 3.1** Considering the final control laws in (20) and the averaged mathematical model presented by equations (5a) and (5b), the dynamic behaviour of the  $k^{th}$  closed loop system, in the  $(e_{1,k}, e_{2,k})$  coordinates, is concluded to be as follows:

$$\begin{pmatrix} \dot{e}_{1,k} \\ \dot{e}_{2,k} \end{pmatrix} = \begin{pmatrix} -\xi_{1,k} & -1/L_b \\ 1/L_b & -\xi_{2,k} \end{pmatrix} \begin{pmatrix} e_{1,k} \\ e_{2,k} \end{pmatrix}. \quad (21)$$

Consequently, it is worth noting that the error variables  $(e_{1,k}, e_{2,k})$  globally exponentially vanish.

### B. Grid current regulator (PFC objective)

The output of the DC-DC boost converters will feed the CHBMI through a DC-link which guarantee the inverters' inputs to be regulated to a given reference. The overall system injects a low THD current with a satisfactory power factor via an LCL filter. This inner-loop is controlled by the backstepping approach; whereas, the outer-loop (DC-link) is controlled via a filtered PI regulator.

#### Step 1

In order to stabilize (7a), the first error between the grid current and its reference is introduced:

$$z_1 = L_{f_2}(x_4 - x_4^*). \quad (22)$$

By differentiating (22) and using (7a), the following tracking error dynamic equation is obtained:

$$\dot{z}_1 = -r_{f_2}x_4 + x_5 - v_g - L_{f_2}\dot{x}_4^*. \quad (23)$$

Based on the fact that an appropriate Lyapunov function must be positive and its time derivative must be negative, the Lyapunov function candidate is chosen as follows:

$$W_1 = 0.5 z_1^2. \quad (24)$$

The time derivative of the Lyapunov function candidate can be written as:

$$\dot{W}_1 = z_1 \dot{z}_1 = -\zeta_1 z_1^2 < 0, \quad (25)$$

where  $\zeta_1$  is a positive design parameter.

Knowing that  $x_5$  is a virtual control input signal and using (24) and (25), the stabilizing function of the subsystem (7a) is written as follows:

$$x_5^* = -\zeta_1 z_1 + r_{f_2}x_4 + v_g + L_{f_2}\dot{x}_4^*. \quad (26)$$

Since  $x_5^*$  does not represent the actual control law, it is needed to introduce the second tracking error defined as:

$$z_2 = C_f(x_5 - x_5^*). \quad (27)$$

Using (27) and replacing by (26), equation (23) becomes:

$$\dot{z}_1 = -\zeta_1 z_1 + z_2/C_f. \quad (28)$$

Thus, time derivative of the selected Lyapunov function results to be:

$$\dot{W}_1 = -\zeta_1 z_1^2 + z_1 z_2/C_f. \quad (29)$$

#### Step 2

To stabilize the subsystem (7b), the second tracking error introduced in (27) needs to be derived as:

$$\dot{z}_2 = x_6 - x_4 - C_f \dot{x}_5^*. \quad (30)$$

A suitable choice of the appropriate Lyapunov function is:

$$W_2 = 0.5 z_2^2 + W_1. \quad (31)$$

The time derivative of the introduced Lyapunov candidate (31) can be expressed:

$$\dot{W}_2 = -\zeta_1 z_1^2 + \left( \dot{z}_2 + \frac{z_1}{C_f} \right) z_2. \quad (32)$$

To guarantee the negativity of the time derivative of  $W_2$ , the following condition must hold:

$$\dot{z}_2 + z_1/C_f = -\zeta_2 z_2 < 0, \quad (33)$$

where  $\zeta_2$  is a positive regulator parameter.

The choice of  $x_6$  as the second virtual control, yields to the second stabilizing function (34) using (30) and (33).

$$x_6^* = -z_1/C_f - \zeta_2 z_2 + x_4 + C_f \dot{x}_5^*. \quad (34)$$

Since  $x_6^*$  is not the actual control law, the third tracking error is defined as:

$$z_3 = L_{f_1}(x_6 - x_6^*). \quad (35)$$

Starting from (35) and using (33) and (34), the dynamics of the second tracking error is given by:

$$\dot{z}_2 = -z_1/C_f - \zeta_2 z_2 + z_3/L_{f_1}. \quad (36)$$

Thus, the time derivative of the Lyapunov function (32) is expressed as follows:

$$\dot{W}_2 = -\zeta_1 z_1^2 - \zeta_2 z_2^2 + z_2 z_3/L_{f_1}. \quad (37)$$

#### Step 3

Stabilizing the subsystem (7c) is the last step to reach the controller's objectives related to the AC side of the structure. The final control laws would ensure the injection of a low THD sinusoidal current to the grid with UPS. For this purpose, let us differentiate the third tracking error:

$$\dot{z}_3 = -r_{f_1}x_6 + \sum_{k=1}^N u_{inv,k}x_{3,k} - x_5 - L_{f_1}\dot{x}_6^*. \quad (38)$$

Taking the following choice of the augmented Lyapunov function into account:

$$W_3 = 0.5 z_3^2 + W_2. \quad (39)$$

Replacing (38) in the time derivative  $W_3$  given by (39), one gets the following form:

$$\dot{W}_3 = -\zeta_1 z_1^2 - \zeta_2 z_2^2 + \left( \dot{z}_3 + \frac{z_2}{L_{f_1}} \right) z_3. \quad (40)$$

Our main interest of forcing the condition below to hold is to ensure the negativity of the time derivative of the augmented Lyapunov function.

$$\dot{z}_3 + z_2/L_{f_1} = -\zeta_3 z_3 < 0, \quad (41)$$

Noting that  $\zeta_3$  is a positive regulator parameter.

It is clearly noticeable that the final control laws appears in the time derivative of the third tracking error. Using this latter and equations (40) and (41), the final control laws can be driven from:

$$\sum_{k=1}^N u_{inv,k}x_{3,k} = -\zeta_3 z_3 + r_{f_1}x_6 + x_5 - z_2/L_{f_1} + L_{f_1}\dot{x}_6^*. \quad (42)$$

**Remark 1** Thanks to the similarity of the H-bridge inverters, it is possible to control them with the same control law.

Assuming so, the final control law expressed by equation (42) can be rewritten as:

$$u_{inv} = \frac{1}{\sum_{k=1}^N x_{3,k}} \left[ -\zeta_3 z_3 + r_{f1} x_6 + x_5 - \frac{z_2}{L_{f1}} + L_{f1} \dot{x}_6^* \right]. \quad (43)$$

**Proposition 3.2** Equation (44) describes the dynamic behaviour of the closed loop system, in the  $(z_1, z_2, z_3)$  coordinates based on the final control law in (43) and the averaged mathematical model presented by equations (7).

$$\begin{pmatrix} \dot{z}_1 \\ \dot{z}_2 \\ \dot{z}_3 \end{pmatrix} = \begin{pmatrix} -\zeta_1 & 1/C_f & 0 \\ -1/C_f & -\zeta_2 & 1/L_{f1} \\ 0 & -1/L_{f1} & -\zeta_3 \end{pmatrix} \begin{pmatrix} z_1 \\ z_2 \\ z_3 \end{pmatrix}. \quad (44)$$

As a conclusion, the error variables  $(z_1, z_2, z_3)$  globally exponentially fade away.

### C. DC-Link voltage regulator

The DC-link plays a vital role in the considered PV system since it feeds the  $N$  H-bridge inverters individually. In this subsection, our interest is directed to providing the multilevel DC-AC converter with DC voltages via regulating the voltages across the DC-link properly and guaranteeing them to closely track a given reference. To this end, the outer loop controller's output is the signal  $\beta$  which is responsible for regulating the sum  $v_b = \sum_{k=1}^N x_{3,k}$  of the DC-link voltages to follow a desired reference  $v_b^*$ . Based on the averaged model (5), (6) and (7) describing the system, and the final control law expressed by equation (43), one can find the relationship between  $\beta$  and  $v_b$  according to the following equation:

$$C_b \dot{v}_b = \sum_{k=1}^N i_{D,k} - N u_{inv,k} x_6, \quad (45)$$

where  $i_{D,k} = (1 - u_{b,k}) x_{2,k}$ , and  $v_b$  denotes the sum of the voltages across the DC-link.

The establishment of the relationship between  $\beta$  and  $v_b$  requires the following assumptions to be taken into account:

- The grid current loop and the PV voltage loops are faster in comparison to the DC-link voltage loop;
- The filter parameters  $L_{f1}, C_f, L_{f2}, r_{f1}, r_{f2}$  are extremely small and, thus, can be neglected.

Knowing that the errors  $(z_1, z_2, z_3)$  vanish exponentially fast and taking the previous assumptions into consideration, the final control law in (43) can be reduced to this expression:

$$u_{inv} = v_g / v_b. \quad (46)$$

As a result, equation (45) can be given by:

$$C_b \dot{v}_b = \sum_{k=1}^N i_{D,k} - \frac{N}{v_b} \beta v_g^2. \quad (47)$$

Based on the principle of power conservation and using the

averaging theory [8], the mathematical equation governing the relationship between  $\beta$  and  $y = \langle v_b^2 \rangle$  is given below:

$$\dot{y} = \psi(t) - \frac{NE^2}{C_b} \beta, \quad (48)$$

where  $\psi(t) = \frac{2}{C_b} \sum_{k=1}^N \langle v_b i_{D,k} \rangle$  and  $y$  are the average values of  $v_b i_{D,k}$  and  $v_b^2$ , respectively.

The signal  $\beta$  represents a control input regulating the quadratic sum of the DC-link capacitors via a filtered PI regulator. This later compares the input reference  $y^*$  and the quadratic sum  $y$  of the  $N$  voltages across the DC-link capacitors so as to generate the control law  $\beta$ . As stated in Remark 1 and taking into consideration that the time derivatives of the signal  $\beta$  must be available up to order 3, the following third order filtered PI regulator is deduced:

$$\beta = L^{-1} \left[ \frac{1}{(1 + \tau s)^3} \left( K_p + \frac{K_i}{s} \right) (Y(s) - Y^*(s)) \right], \quad (49)$$

where  $L^{-1}$  designates the well-known inverse Laplace transform,  $\tau$ ,  $K_p$  and  $K_i$  are positive design parameters.

## IV. SIMULATION

This section is devoted to the simulation of the studied system so as to prove its efficacy, robustness and ability to face faulty conditions. The simulation is implemented in MATLAB/SIMULINK/ SimPowerSystems environment. The theoretical results are validated via choosing the described system (Fig. 1.) to be tested on  $N = 3$ , i.e., three individual PV arrays (1Soltech 1STH-220-P) which contain four parallel strings including two series-connected modules each. Each of the PV arrays supply a DC-DC boost converter connected to a DC-link individually. On the AC side, there are three CHBMI connected to the electrical grid via an LCL filter. The following tables represent the system and controller parameters.

TABLE I

PLANT SYSTEM PARAMETERS

Parameters	Symbols	Values
Network	$v_g, f_n$	220 V /50 Hz
Boost	$C_{pv}, L_b, r_b$	100 $\mu$ F, 3 mH, 50 m $\Omega$
DC Link capacitors	$C_b$	1 mF
LCL filter	$L_{f1}, C_f, L_{f2}, r_{f1} = r_{f2}$	0.3 mH, 100 $\mu$ F, 0.1 mH, 50 m $\Omega$
Carrier frequency	$F_{PWM}$	10 kHz

TABLE II

CONTROLLER PARAMETERS

Parameters	Symbols	Values
PV voltage regulator	$\xi_{1,k}, \xi_{2,k}$	10, 3000
Grid current regulator	$\zeta_1, \zeta_2, \zeta_3$	$5.10^3, 20.10^3, 336.10^3$
DC Link regulator	$K_p, K_i, \tau$	$5.10^{-4}, 4.10^{-3}, 10ms$

The controlled system goes through three performance checking tests. In the first one, we examine its performance vis-à-vis mismatching PV irradiations. In the second one, we evaluate the results related to equal PV irradiations,

and lastly, we investigate the system's failure tolerance. The results of these tests are presented in Figure 3.

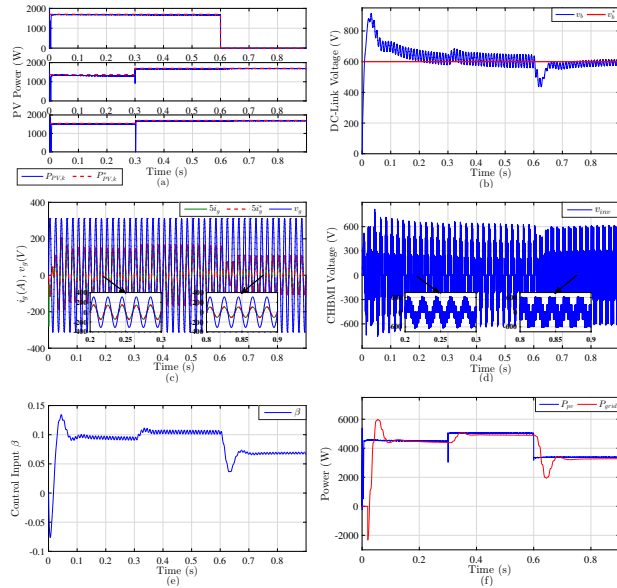


Fig. 3. (a) PV powers and their references, (b) The sum of the DC-Link voltages and its reference, (c) The output of the CHBMI, (d) PFC checking, (e) The control signal  $\beta$ , (f) PV and grid powers.

#### A. Performance test 1: Mismatching Irradiations Mode

This test aims at checking the controlled system performance while the PVs are operating under different irradiation conditions in the time interval  $[0s, 0.3s]$ , with respect to the following patterns: PV1:  $1000W/m^2$ , PV2:  $800W/m^2$ , and PV3:  $900W/m^2$ ; whereas, the temperature is kept unchanged ( $25^\circ C$ ). The above patterns correspond to a power generation of  $1703W$  for PV1,  $1374W$  for PV2 and  $1539W$  for PV3.

#### B. Performance test 2: Matching Irradiations Mode

In this test, we suppose that all the PV panels operate under the same irradiations and temperature ( $1000W/m^2$ ,  $25^\circ C$ ), in the time interval  $[0.3s, 0.6s]$ .

#### C. Performance test 3: Fault Mode

The third test evaluates the performance of the system facing a failure either in the PV panels or in the DC-DC boost converters at the time interval  $[0.6s, 0.9s]$ . As a consequence, the failing subsystem is totally disconnected, and thus does not provide the needed power.

Figure 3 proves that the controlled objectives are successfully achieved in the three previously described modes. To clarify more, Figure 3.a demonstrates that the MPPT objective is guaranteed since each PV source operates at its optimal power point that correlates with the received irradiations. Figure 3.b shows that the DC-link voltage regulation is guaranteed, in the mean, regardless of the PV irradiation variations or the occurring defect at the level of PV1. The efficacy of the controller is clearly seen in Figure 3.c, where the grid current follows its reference tightly in the three modes, assuring this way a satisfactory power factor correction. To check the THD of the injected grid current,

an FFT analysis has been performed revealing that the grid current distortion is around 1.52%. This value complies with the standard norms (the Australian standard (AS-4777-2005) and IEEE 929-2000 standard (IEEE-929-2000)) [9], which restrict a current's THD to be less than 5%. Figure 3.d represents the CHBMI voltage. Since the simulation occurs on three CHBMI, a seven level voltage is generated in the first and second mode. For the third mode that is characterized by the failure, and thus the absence of a voltage source, the H-bridges deliver only a five level voltage. The control law  $\beta$  provided by the filtered PI regulator is depicted in Figure 3.e. This signal is bounded and correlates with the grid current magnitude, the grid power and the PV irradiations. The small ripples appearing in this signal are due to the power factor correction (PFC) properties. In Figure 3.f, the power generated by the PVs and the one absorbed by the electrical grid through the power-conditioning unit are equal, in the mean, which reflects that the energy conservation principle.

## V. CONCLUSIONS

This paper has tackled the study of a complete PV-fed DC-AC conversion system based on a CHBMI. The used multi-loop regulator demonstrates its efficacy in reaching the control objectives in terms of extracting the maximum available PV power, DC-link regulation and power factor correction. The whole controlled system can work under the same or mismatching climate conditions and proved to be able to tolerate failures and operate under faulty conditions.

## REFERENCES

- [1] K. Wang, X. Wu, F. Liu, Y. Wang, and R. Zhu, "Cascaded H-bridge multilevel converter topology for large-scale photovoltaic system with balanced operation," in IECON 2017 - 43rd Annual Conference of the IEEE Industrial Electronics Society, Beijing, Oct. 2017, pp. 6452–6457.
- [2] H. Katir, A. Abouloifa, K. Noussi, I. Lachkar and F. Giri, "Cascaded H-bridge Inverters for UPS Applications: Adaptive Backstepping Control and Formal Stability Analysis," in IEEE Control Systems Letters, doi: 10.1109/LCSYS.2021.3051875.
- [3] A. Lashab et al., "A Cascaded H-Bridge With Integrated Boosting Circuit," IEEE Trans. Power Electron., vol. 36, no. 1, pp. 18–22, Jan. 2021.
- [4] C. Boonmee and Y. Kumsuwan, "Control of single-phase cascaded H-bridge multilevel inverter with modified MPPT for grid-connected photovoltaic systems," in IECON 2013 - 39th Annual Conference of the IEEE Industrial Electronics Society, Vienna, Austria, Nov. 2013, pp. 566–571.
- [5] H. Katir, A. Abouloifa, K. Noussi, and I. Lachkar, "Sliding Mode Based Control of Five Cascaded H-Bridge Inverters," in 2020 International Conference on Electrical and Information Technologies (ICEIT), Rabat, Morocco, Mar. 2020, pp. 1–6.
- [6] K. Javed, H. Ashfaq, and R. Singh, "An improved MPPT algorithm to minimize transient and steady state oscillation conditions for small SPV systems," IJRED, vol. 7, no. 3, pp. 191–197, Dec. 2018.
- [7] A. Abouloifa, C. Aouadi, I. Lachkar, Y. Boussairi, M. Aourir, A. Hamdoun, "Output-Feedback Nonlinear Adaptive Control Strategy of the Single-Phase Grid-Connected Photovoltaic System," Journal of Solar Energy, 1–14, 2018.
- [8] A. Abouloifa, F. Giri, I. Lachkar, F. Z. Chaoui, M. Kissauoui, and Y. Abouelmahjoub, "Cascade nonlinear control of shunt active power filters with average performance analysis," Control Engineering Practice, vol. 26, pp. 211–221, May 2014.
- [9] Y. Du, D. D.-C. Lu, G. James, and D. J. Cornforth, "Modeling and analysis of current harmonic distortion from grid connected PV inverters under different operating conditions," Solar Energy, vol. 94, pp. 182–194, Aug. 2013.